Drag Reduction and Turbulent Structure in Two-Dimensional Channel Flows

K. J. Harder and W. G. Tiederman

Email alerting service   Receive free email alerts when new articles cite this article - sign up in the box at the top right-hand corner of the article or click **here**

To subscribe to *Phil. Trans. R. Soc. Lond. A* go to:
http://rsta.royalsocietypublishing.org/subscriptions

Drag reduction and turbulent structure in two-dimensional channel flows

By K. J. Harder† and W. G. Tiederman

School of Mechanical Engineering, Purdue University, West Lafayette, Indiana 47907, U.S.A.

A two-component laser velocimeter has been used to determine the effect of wall strain rate, polymer concentration and channel height upon the drag reduction and turbulent structure in fully developed, low concentration, two-dimensional channel flows. Water flows at equal wall shear stress and with Reynolds numbers from 14430 to 34640 were measured for comparison. Drag reduction levels clearly depended upon wall strain rate, polymer concentration and channel height independently. However, most of the turbulent structure depended only upon the level of drag reduction. The slope of the logarithmic law of the wall increased as drag reduction increased. Similarly, the root-mean-square of the fluctuations in the streamwise velocity increased while the r.m.s. of the fluctuations in the wall-normal velocity decreased with drag reduction. The production of the streamwise normal Reynolds stress and the Reynolds shear stress decreased in the drag-reduced flows. Therefore it appears that the polymer solutions inhibit the transfer of energy from the streamwise to the wall-normal velocity fluctuations. This could occur through inhibiting the newtonian transfer mechanism provided by the pressure-strain correlation. In six drag-reducing flows, the sum of the Reynolds stress and the mean viscous stress was equal to the total shear stress. However, for the combination of highest concentration (5 p.p.m.), smallest channel height (25 mm) and highest wall strain rate (4000 s^{-1}), the sum of the Reynolds and viscous stresses was substantially lower than the total stress indicating the presence of a strong non-newtonian effect. In all drag-reducing flows the correlation coefficient for uv decreased as the axes of principal stress for the Reynolds stress rotated toward the streamwise and wall-normal directions.

---

1. Introduction

During the past 40 years there have been numerous studies of drag reduction with polymer additives. Despite some very successful applications of the technique such as in the Trans Alaskan Pipeline (Motier & Carrier 1989), a complete understanding of this phenomena has been elusive. Recent reviews by Lumley & Kubo (1985) and Tiederman (1990) show that efforts to determine an appropriate set of dimensionless parameters for the dependent variables in drag-reducing flows have not yet been successful. The primary reason for this lack of success is the absence of rheological measurements and/or theory that accurately describe the elastic and elongational properties of dilute polymer solutions.

There is widespread belief that the wall strain rate, channel height, polymer

---

† Present address: Cummins Engine Company, M/C 50182 Box 3005, Columbus, Indiana 47202–3005, U.S.A.

concentration and polymer-solvent combination (Berman 1978) are among the variables that strongly influence the amount of drag reduction achieved. However, there have not been any systematic studies of the combined influence of these variables upon the drag-reduced flow fields. The primary object of this study was to systematically determine the influence of the first three of these variables for aqueous solutions of the polyacrylamide Separan AP 273.

Two channels with heights of 25 and 60 mm were used to simultaneously study the two-component velocity field and the pressure drop-flow rate characteristics for 3–5 p.p.m. (parts per million by mass), well mixed, fully developed, drag-reducing flows over a range of wall strain rates from 1000 to 4000 s^{-1}. For comparison, measurements were also made at the same wall strain rates in four water flows yielding data over a Reynolds number range from 14 430 to 34 640. The Reynolds number, Re_h, is based on channel height, h, and the bulk average velocity.

The two dimensional channel flow offers several advantages for drag reduction studies with polymer additives. Optical access for flow visualization and laser velocimetry is relatively easy, fully developed conditions can be achieved and pressure drop measurements show immediately whether or not the viscous drag has been reduced. In addition, as documented by Kline (1990), Kline & Robinson (1990), and Robinson (1991), the turbulent structure of newtonian two-dimensional channel flows has been well studied. The principal disadvantages compared with pipe flow facilities are that long, high aspect ratio channels are more difficult to build and maintain and the Reynolds number range with a given pump or blower is less. As a result turbulent structure studies in drag-reducing flows have been conducted over a limited Reynolds number range in channels while the flow rate-pressure drop characteristics have been documented over a wider range of conditions in circular pipes.

In this study emphasis was placed on flow characteristics very near the wall because beginning with the study of Wells & Spangler (1967) it has been found that the polymer must be in the near-wall region for drag reduction to occur. Wu & Tulin (1972) obtained similar results in a flat plate boundary layer. McComb & Rabie (1982) showed that drag reduction occurs only when polymer is present in the buffer zone of turbulent wall flows. Tiederman *et al.* (1985) verified that drag reduction does not occur when polymer is confined to the viscous sublayer.

A primary goal of drag-reduction research is to model the flow so that the pressure drop can be predicted given a flow condition and configuration. For example Granville (1985) proposed a method for predicting drag reduction in one pipe based on results in another pipe. In this method, the slope of the logarithmic portion of the mean velocity is assumed to be constant. This assumption is not always valid as will be seen from the results of this study.

Another objective was to verify the results of Willmarth *et al.* (1987), who reported a significant decrease in the Reynolds shear stress, $\overline{uv}$ for a channel flow of a dilute polyethylene oxide solution. The decrease was large enough that the sum of the viscous and Reynolds shear stress did not add up to the time-average shear stress. Therefore, they proposed the existence of an additional retarding force in polymer flows.

In this study the polymer was injected far enough upstream (greater than 30 channel heights) so that the polymer was well mixed at the measurement location. The channels were also over 100 channel heights long so the flow was clearly fully developed at the measurement station. Since the well-mixed polymer concentrations

were very low (3–5 p.p.m.), the shear viscosity for the drag-reduced flows and a water flow were essentially the same. A factorial design (see Hunter 1960) was used to determine the dependence of the quantities of interest upon wall strain rate and average polymer concentration. A two-component laser Doppler velocimeter was used to make the velocity measurements.

2. Apparatus and procedures

2.1. *Experimental facilities*

The experiments were performed in a recirculating water flow loop that was driven by one to four centrifugal pumps operating in parallel. Stilling tanks at each end of the channel test sections isolated the channels from hydrodynamic disturbances of the flow loop, provided a smooth entrance flow, and contained a cooling coil to maintain the water at a constant temperature (see Tiederman *et al.* 1985).

Two rectangular channels were used. The larger of the two channels was 6.0 cm high by 57.5 cm wide and over 100 channel heights long. Polymer solutions were injected through flush-mounted angled slots that were located over 40 channel heights upstream of the test location. The smaller of the two channels was 2.5 cm high by 25 cm wide and was *ca.* 190 channel heights long. When this smaller channel was in place, a removable contraction section was inserted into the outlet of the upstream tank to reduce the flow area from $6.0 \times 57.5 \text{ cm}^2$ to $2.5 \times 25 \text{ cm}^2$. The injection slots for this channel were located 100 channel heights upstream of the test location. For both channels, the polymer solutions were well mixed with the channel water at the test locations.

The pressure gradient in the test section was determined using a micrometer manometer with carbon tetrachloride as the working fluid. The sensitivity of the pressure drop measurements with this manometer was 0.015 mm of water.

2.2. *Laser Doppler velocimeter*

A three-beam, two-colour, laser Doppler velocimeter was used to obtain two-component velocity data. The system included 40 MHz frequency shifting with electronic down mixing, a 2.27 beam expander, and a 250 mm focusing lens. The scattered light was collected off the optical axis in order to obtain finer spanwise spatial resolution. The two-component data were acquired at $\pm 45°$ to the streamwise flow direction so that measurements could be made very near the wall and so that the error in the $\overline{uv}$ measurements would be minimized.

Output from the photomultiplier tubes was filtered and processed using two TSI model 1980 counter processors. A coincidence window ensured that data from both processors were from the same particle. The data were sampled at equal time intervals to remove velocity bias. Time-average statistics were calculated from records of 10 000 independent realizations.

2.3. *Data analysis*

From the orthogonal pair of velocities, U_1 and U_2, which are the velocities measured at $\pm 45°$ from the flow direction, the streamwise and normal velocity components were determined. For any angle θ measured relative to the flow direction, the streamwise and normal velocity components are given by

$$U = U_2 \cos \theta + U_1 \sin \theta, \tag{1}$$

$$V = U_2 \sin \theta - U_1 \cos \theta. \tag{2}$$

In this study θ was determined such that time average $\bar{V}$ from equation (2) was zero in the outer flow where signal quality was best. This single value of θ was used for all y-locations.

The equations for the second moments are:

$$\overline{u^2} = \overline{u_1^2}\sin^2\theta + \overline{u_2^2}\cos^2\theta + 2\overline{u_1 u_2}\cos\theta\sin\theta, \tag{3}$$

$$\overline{v^2} = \overline{u_1^2}\cos^2\theta + \overline{u_2^2}\sin^2\theta - 2\overline{u_1 u_2}\cos\theta\sin\theta, \tag{4}$$

$$\overline{uv} = [\overline{u_2^2} - \overline{u_1^2}]\sin\theta\cos\theta + \overline{u_1 u_2}[\sin^2\theta - \cos^2\theta]. \tag{5}$$

Near the wall the calculation for the wall normal normal-stress is influenced most by noise. This occurs because the sum of the first two terms in equation (4) is very close in value to the third term. Thus a fixed amount of error (optical noise, electronic noise) will cause larger percentage of error in the subtraction of the third term from the sum of the first two. In the first term of equation (5), the difference between $\overline{u_2^2}$ and $\overline{u_1^2}$, is relatively large. These factors yield a more accurate estimate of $\overline{uv}$ than $\overline{v^2}$. The calculation of $\overline{u^2}$ is relatively insensitive to noise.

The average wall shear stress, $\bar{\tau}_w$, in a fully developed flow is proportional to pressure drop or

$$\bar{\tau}_w = (\Delta P/\Delta x)\,a. \tag{6}$$

Here $\Delta P/\Delta x$ is the pressure gradient, $a = \frac{1}{2}h$, and h is the channel height. However, in a rectangular channel, the wall shear stress is not constant along the perimeter at any given cross section. Hence the shear stress in the vicinity of the test location will differ from the average shear stress. To make a more accurate estimate of the local wall shear stress, two-component velocity data were used. For fully developed, newtonian flows, the shear stress is equal to the sum of the viscous and Reynolds stress and varies linearly from the wall to the centreline. Therefore,

$$\tau = \mu\,\mathrm{d}\bar{U}/\mathrm{d}y - \rho\overline{uv} = \tau_w(1 - y/a), \tag{7}$$

where τ is the total shear stress at a point in the flow, and τ_w is the local wall shear stress. Therefore, the shear velocity, $u_\tau = (\tau_w/\rho)^{\frac{1}{2}}$ may be estimated from

$$u_\tau = [(\nu\,\mathrm{d}\bar{U}/\mathrm{d}y - \overline{uv})/(1 - y/a)]^{\frac{1}{2}} \tag{8}$$

when the turbulent shear stress, $\overline{uv}$ and is measured and the derivative of the mean velocity is calculated from the data. Equation (8) yields an estimate of the wall shear velocity at the midspan of the channel where the flow is not affected by the secondary flows in the corners. Since the well mixed concentration of polymer in the channel is low (3–5 p.p.m.), the difference in the shear viscosities of water and polymer flows cannot be measured. Therefore, water properties were used in all calculations. Figure 1 illustrates how data from all y-locations was used to estimate u_τ for the water flow in the 2.5 cm channel at a wall strain rate of 1000 s^{-1}. The shear velocity, estimated as the average of all of the points, had a value of $0.0294\text{ m s}^{-1} \pm 0.0017\text{ m s}^{-1}$ at 95% confidence.

2.4. *Factorial design*

To estimate the dependence of drag reduction upon wall strain rate and average polymer concentration in the channel, a factorial design was implemented. This statistical method is described by Hunter (1960) and has the advantage of providing the required result with the minimum number of experiments. For this study, the
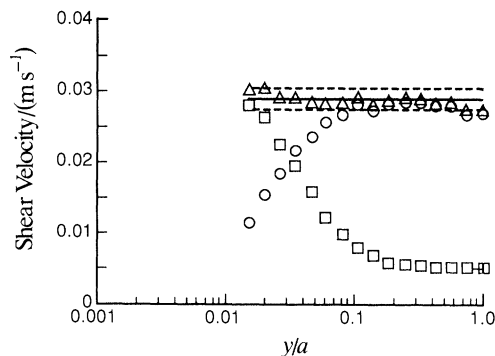
Figure 1. Estimated shear velocity for water flow, wall strain rate $= 1000$ s^{-1}, 2.5 cm channel: $\triangle$, u_τ; $\square$, viscous contribution; $\bigcirc$, turbulent contribution; $= = = =$, 95 % confidence interval; ——, u_τ mean.

Table 1. *Experimental conditions for the factorial design*

X_1	X_2	$(\mathrm{d}\bar{U}/\mathrm{d}y)|_\mathrm{w}/\mathrm{s}^{-1}$	$\bar{C}$ (p.p.m.)
-1	-1	1000	3
-1	1	1000	5
0	0	2500	4
1	-1	4000	3
1	1	4000	5

independent variables were the wall strain rates, which varied from 1000 to 4000 s^{-1} and the well-mixed polymer concentrations which varied from 3 to 5 p.p.m. The normalized independent variables are defined by

$$X_1 = \{(\mathrm{d}\bar{U}/\mathrm{d}y)|_\mathrm{w} - 1500 \text{ s}^{-1}]/2500 \text{ s}^{-1} \tag{9}$$

and

$$X_2 = (\bar{C} - 4 \text{ p.p.m.})/1 \text{ p.p.m.} \tag{10}$$

Experimental conditions for the factorial design are shown in table 1.

3. Results

3.1. *Effect of wall strain rate and polymer concentration on drag reduction*

Pressure drop measurements at each of the flow conditions specified in the factorial design yielded the drag reduction results shown in figure 2. The percent drag reduction, D_R, is based on the decrease in pressure drop at a constant flow rate. Due to limited pumping capacity, data could only be obtained in the 6.0 cm channel at a wall strain rate of 1000 s^{-1}. Since the regression analysis requires data at all values of the independent variables, only the 2.5 cm channel data could be used to evaluate the effect of wall strain rate and concentration. The flow condition corresponding to the non-dimensional origin of the design space was repeated several times to estimate the error involved in the measurement. A linear dependence of percent drag reduction upon the independent variables was assumed, and a least-squares regression analysis yielded the model:

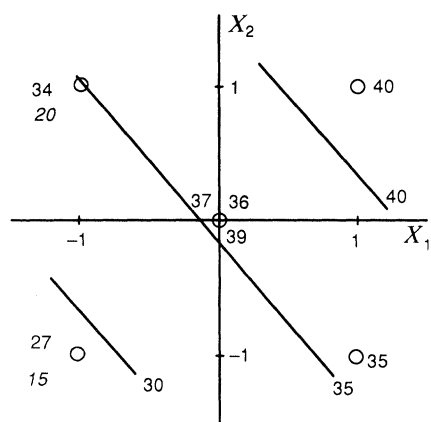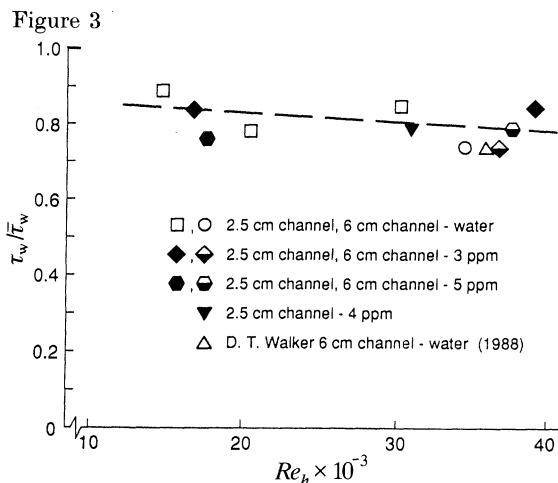$$D_\mathrm{R} = 35.4 + 3.5X_1 + 3.0X_2 - 0.5X_1 X_2. \tag{11}$$

Figure 2

Figure 3

Figure 2. Dependence of drag reduction upon wall strain rate and polymer concentration; linear model: italicized numbers, 6.0 cm channel results; other, 2.5 cm channel results.

Figure 3. Effect of Reynolds number on the ratio of local to average shear stress.

An F-test revealed that the influence of the cross correlation term is not larger than the error of measurement. Hence the $X_1 X_2$ term is not significant and the linear model becomes:

$$D_R = 35.4 + 3.5 X_1 + 3.0 X_2. \tag{12}$$

This model yields a correlation coefficient coefficient of 0.9986. Isocontours from the model are shown on figure 2.

   Results from the 6.0 cm channel (shown as italicized numbers on figure 2) show that for the same wall strain rate and polymer concentration, the drag reduction is different in the two channels. From these results, it is seen that drag reduction clearly depends upon all three variables, although the functional dependence upon channel height was not determined in this study.

3.2. *Wall shear stress*

   It is of primary importance to have an accurate value of wall shear stress. For this study, equations (6) and (7) estimate wall shear stress (hence shear velocity) from pressure drop and from the sum of the viscous and Reynolds stresses respectively. Figure 3 shows the relationship between the local wall shear stress, τ_w, and the average wall shear stress, $\bar{\tau}_w$. In all flows, $\bar{\tau}_w$ was from 10–25 % higher than τ_w. It is hypothesized that end-wall effects are responsible for the significant difference in the shear stress estimates. Because of the difference in the local and average shear stresses, the local shear stress, τ_w, was used to normalize the velocity statistics. It is not only the best estimate of the shear stress at the mid-span of the channel, but it also is independent of the channel aspect ratio.

   For all but one of these dilute, well-mixed polymer flows, the newtonian assumption shown in equation (7) was valid. However, for the drag-reduced flow at $4000\ \mathrm{s^{-1}}$ and 5 p.p.m. in the 2.5 cm channel, a plot such as figure 1 yielded such widely scattered values for the shear velocity that a good average was impossible to estimate. Willmarth *et al.* (1987) obtained similar results for their drag-reducing channel flow. Apparently some non-newtonian factor is involved and equation (8)

cannot be used to estimate τ_w. Therefore a line was fit through the data on figure 3; a value for the ratio of the stresses for the 4000 s^{-1}, 5 p.p.m. flow ($Re_h = 41\,610$) was extrapolated and τ_w was estimated from the measured pressure drop. This was done so that the velocity statistics for all flows can be normalized in the same way.

3.3. *Water flows*

Velocity measurements were made for water flows at each of the wall strain rates in the experimental design (three in the 2.5 cm channel and one in the 6.0 cm channel). These measurements were made to verify the standard nature of these flows and to have a base for comparison with drag-reduced flows.

The newtonian, two-dimensional, fully developed flow has been well studied. Kreplin & Eckelmann (1979) measured the three fluctuation velocity components in an oil channel, where due to the high viscosity of the oil, they obtained excellent spatial resolution. Hussain & Reynolds (1975) made streamwise velocity measurements in an air channel flow with an exceptionally large development length ($l/h = 196$) and large aspect ratio (18:1). Previous measurements in these 2.5 cm and 6.0 cm channels were reported by Luchik & Tiederman (1988) and Walker & Tiederman (1990) respectively.

Figure 4 shows the behaviour of the root-mean-square (r.m.s.) of the fluctuating streamwise and normal velocities as a function of distance from the wall. These results show that in all of the water flows, u'^+ peaks at 2.76 for a $y^+ \approx 15$. The superscript '+' indicates that the variable has been made dimensionless by using inner variables, u_τ and ν. The r.m.s. of the normal velocity peaks at a $y^+ \approx 75$ with a value of 1.12. For $y^+ > 100$, these results agree with those of Wei & Willmarth (1989) who show that the fluctuating quantities in the outer region do not scale with inner variables and that there is a Reynolds number dependence. However, in contrast with Wei & Willmarth, inner scaling does correlate the data for all Reynolds number in the wall region ($y^+ < 50$). The results of this study show similar trends as those of Walker & Tiederman (1990) but are about 7% lower across the channel half-height. These results agree well in trend with the numerical simulation of Kim *et al.* (1987) and the experiments of Hussain & Reynolds (1975) but the values here are about 7% higher.

As described in §2.3, measurement of v' is adversely affected by noise. For this counter processor, the proper parameter for this effect is the Schmitt-trigger threshold-to-noise ratio. When the threshold to noise ratios was less than 4, v' would increase as the wall was approached rather than decrease. The u' measurements were unaffected by signals with threshold-to-noise ratios less than four and the uv data were somewhat sensitive but not to the same extent as v'. Therefore, no data are presented that did not meet or exceed a threshold-to-noise ratio of four.

As shown by Harder (1989) all of the near-wall u'^+ data agree very well with data from Kreplin & Eckelmann (1979). There is some scatter in the v'^+ data for $y^+ < 10$ and the results are higher than expected from Finnicum & Hanratty (1985) who show that v'^+ should vary as y^{+2} as y^+ goes to zero. For $y^+ > 10$, the near-wall v'^+ results agree well with those of Kreplin & Eckelmann (1979).

Figure 5 shows the $\overline{uv}$ data from the water flow in semi-log coordinates, which allows closer inspection of the near-wall region. These results show that as the wall strain rate (Reynolds number) increases, a region in y^+ develops where the turbulent stress is essentially constant for each flow. The higher Reynolds number flows show such a region, while the lower Reynolds number flows do not. This is the constant
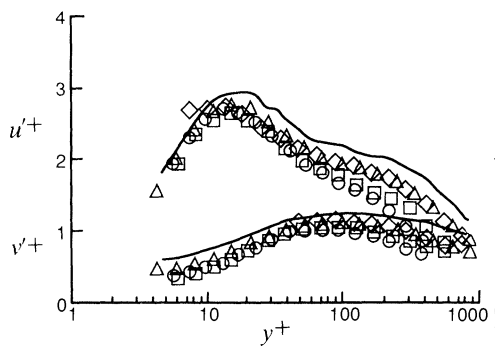
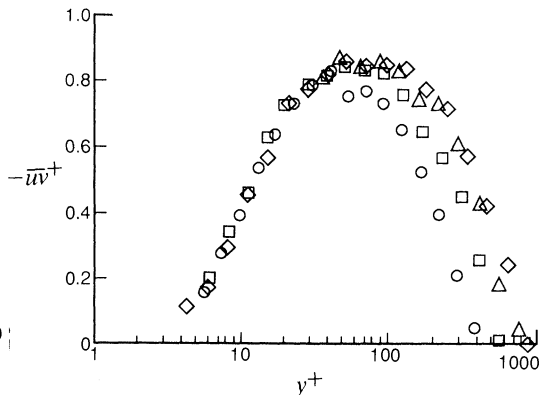Figure 4   Figure 5

Figure 4. Root-mean-square velocity fluctuation profiles for water flows: $\circ$, 2.5 cm channel, $Re_h = 14430$; $\square$, 2.5 cm channel, $Re_h = 20260$; $\diamond$, 2.5 cm channel, $Re_h = 30420$; $\triangle$, 6.0 cm channel, $Re_h = 34640$; ——, fit to results of Walker & Tiederman (1990).

Figure 5. Near-wall behaviour of the Reynolds shear stress: $\circ$ 2.5 cm channel, $Re_h = 14430$; $\square$ 2.5 cm channel, $Re_h = 20260$; $\triangle$ 2.5 channel, $Re_h = 30420$; $\diamond$, 6.0 cm channel, $Re_h = 34640$.

stress region that Sreenivasan (1989) uses to define the logarithmic zone of the mean velocity profile. It is important to note that the constant stress region is not a stringent condition for a logarithmic zone, especially at low Reynolds number. Sreenivasan points out that a region where the Reynolds stress is at least 70 % of the peak can be used to determine the log zone without losing accuracy. Again notice that for $y^+ < 50$, inner scaling correlates the data very well for all Reynolds number.

The correlation coefficient, R_{uv}, decreases with increasing Reynolds number, a trend in agreement with Wei & Willmarth (1989) (see Harder 1989). The peak decreases from 0.43 to 0.37 as the Reynolds number increases from 14430 to 30640. The present results agree with the numerical work of Kim *et al.* (1987) who obtained a peak value of about 0.45 at a Reynolds number *ca.* 5600.

3.4. *Drag-reduced flows*

Two-component velocity measurements were made at each of the flow conditions in the factorial experimental design. Most of the drag-reducing flows differ from the water flows in the same general way. However, as mentioned in §3.2, the viscous and Reynolds stresses did not add up to the total shear in the region of $y^+ < 100$ for the drag-reduced flow at 4000 s^{-1} and 5 p.p.m. The results presented here include those of a typical drag-reduced flow (1000 s^{-1}, 3 p.p.m.) and those of the strongly non-newtonian flow (4000 s^{-1}, 5 p.p.m.) so that the similarities and differences of this strongly non-newtonian flow can be seen. Both experiments were conducted in the 2.5 cm channel. Other polymer data were used to establish trends for the profile deviations. The kinematic viscosity used for normalization of the drag-reduced flows was that of water at 22 °C, which is 0.96×10^{-6} m^2 s^{-1}. Results from the other flow conditions are presented in Harder (1989).

3.4.1. *Mean velocity*

Figure 6 shows the effect of polymer addition upon the mean velocity profile. As shown by Reischman & Tiederman (1975), the buffer zone thickens and offsets the logarithmic zone correspondingly. As can be seen, the results from the typical flow
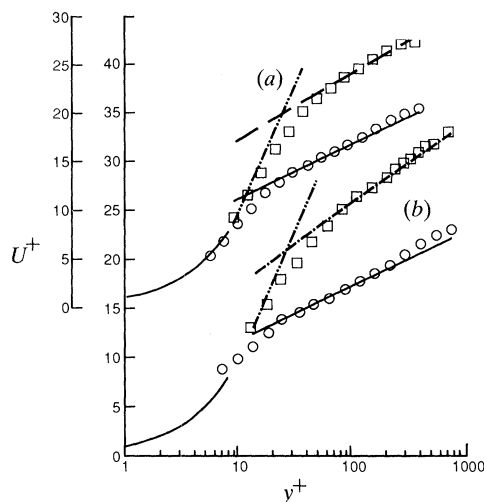
Figure 6

Figure 7

Figure 6. Mean velocity profiles: (*a*) typical drag-reduced flow; (*b*) strongly non-newtonian drag-reduced flow; □, drag-reduced data; ○, water flow data at equal wall shear; ——, standard law of the wall; –––, —·—, fitted law of the wall; —··—, Virk ultimate asymptote.
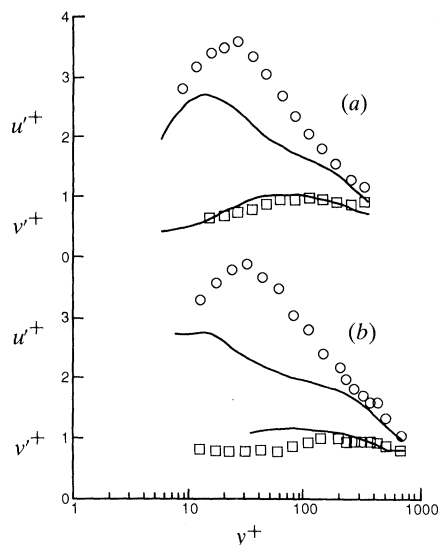
Figure 7. Root-mean-square velocities: (*a*) typical drag-reduced case; (*b*) strongly non-newtonian drag-reduced case; ○, u'^{+}; □, v'^{+}; ——, fit to water flow results at equal τ_{w}.

and the strongly non-newtonian flow agree in trend, although the slopes and offsets of the two logarithmic regions vary. If a straight line could be drawn through at least four data points for $50 < y^{+} < 300$ plotted in semi-log u^{+}, y^{+} coordinates, a logarithmic region was assumed to exist. A regression analysis performed with these data yielded the slope, $1/\kappa$, and the intercept, B, of the log-law, $U^{+} = (1/\kappa) \ln y^{+} + B$. This form of the log-law was assumed to hold for all drag-reduced flows. Coles (1968) suggests that this method is as good as any in determining the log-law constants. As can be seen on figure 6, the fitted line (dashed) agrees with the data in the outer flow.

Since definition of the log zone can be somewhat subjective, other experiments have assumed that the slope is the same for water flows and drag-reduced flows. This assumption creates the idea of a parallel shift upward of the log zone in drag-reduced flows. However, for the data in the present study, if the slope is held constant, the fitted line will not pass through more than two data points. The constant κ was found to have a linear dependence upon the amount of drag reduction given by

$$\kappa = 0.41 - 0.03 D_{\mathrm{R}}. \tag{13}$$

Since the slope changed with drag reduction, Granville's method (1985) for scale-up based on constant slope will not work well for these flows.

3.4.2. *Second moments*

Figure 7 shows a comparison of the streamwise and wall-normal, r.m.s., velocities of the 3 p.p.m. polymer flow with a water flow, both at a wall strain rate of 1000 s^{-1}. The peak in u'^{+} broadens and moves outward from $y^{+} = 15$ to $y^{+} = 30$. These results agree in trend with those of Luchik & Tiederman (1988) and Reischman & Tiederman (1975). The peak in u'^{+} is about 12 % higher than both Luchik & Reischman's value
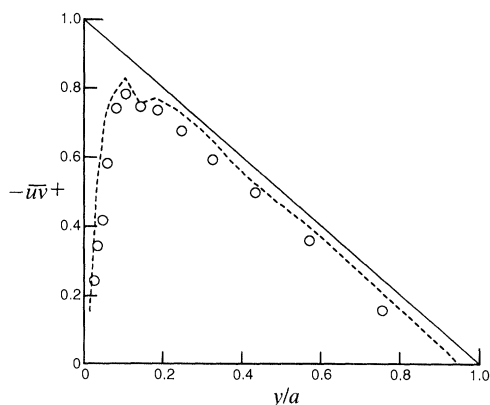
Figure 8   Figure 9

Figure 8. Reynolds shear stress distribution; ○, typical drag-reduced flow; – – – –, fit to water flow data at equal wall shear stress; ——, $(1 - y/a)$.
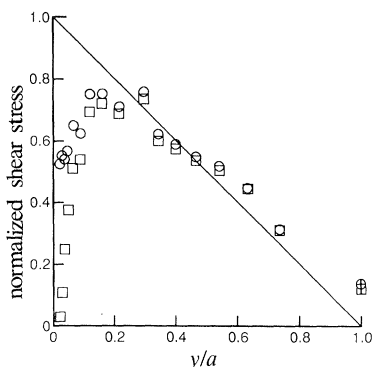
Figure 9. Difference between the shear stress as estimated by the sum of the viscous and Reynolds stresses and by the streamwise pressure gradient for strongly non-newtonian flow case: □, Reynolds shear stress; ○, sum of Reynolds and viscous shear stresses; ——, $(1 - y/a)$.

but it agrees with the measurements of McComb & Rabie (1982). For $y^+ < 100$, the drag-reduced flow shows a damping of v'^+ which is consistent with the results of Luchik & Tiederman (1988). As in the water flow cases, the v' results for $y^+ \leqslant 10$ appear to be high and are therefore questionable. As in the case of the mean velocity profiles, the typical and strongly non-newtonian flows had similar trends in the r.m.s. velocities. All other 2.5 cm channel drag-reduced results exhibited the same trends, although some results showed more scatter in v'. The 6.0 cm channel results were similar in trend to those of the 2.5 cm channel, but since the drag reduction was low, the change in the statistics was not as pronounced.

The turbulent shear stress distribution for the typical drag-reduced flow is shown in figure 8 with the corresponding water flow at equal wall shear stress. This plot shows that the turbulent stress in drag-reduced flows follows the same trends as in the water flow. This supports the assumption that many drag-reduced flows are still basically newtonian flows.

The 2.5 cm channel flow at a wall strain rate of 4000 s^{-1} and average polymer concentration of 5 p.p.m. failed to yield an accurate measurement of τ_w as calculated by equation (7). This strongly non-newtonian flow exhibited the same phenomenon as reported by Willmarth *et al.* (1987). These features are namely that $\overline{uv}$ behaves as the other drag-reduced flows in the outer portion of the flow. However, as the wall is approached ($y^+ < 100$), $\overline{uv}$ rapidly decreases and the sum of $-\rho\overline{uv}$ and $\mu \, \mathrm{d}\bar{U}/\mathrm{d}y$ does not equal τ. Figure 9 shows the difference between the sum of the viscous and Reynolds stress and the local shear stress estimated from figure 3 and the streamwise pressure gradient.

The profile of the correlation coefficient, R_{uv}, for the typical drag-reduced flow is shown compared with the R_{uv} for water flow at equal wall shear stress in figure 10. Throughout the whole flow régime, the correlation coefficient is about 25% lower than the water flow values. In plots of the correlation coefficient the difference in behaviour of the Reynolds stresses is evident for the flow condition with a wall strain rate equal to 4000 s^{-1} and average polymer concentration of 5 p.p.m. The
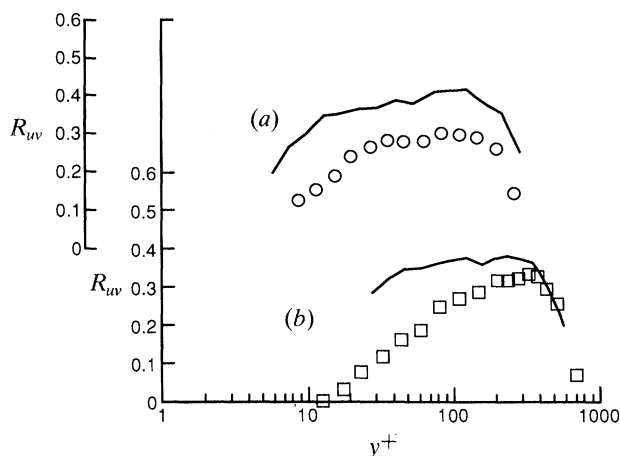
Figure 10. Correlation coefficient distribution: (*a*) ○, typical drag-reduced flow; (*b*) □, strongly non-newtonian drag-reduced flow, ——, fit to water flow data at equal τ_w.

correlation coefficient behaves as the typical drag-reduced case in the outer flow, but for $y^+ < 100$ the correlation decreases rapidly as the wall is approached. All other drag-reduced flows behave as the typical case, although the degree of difference between the polymer and water flows may vary. The typical trend agrees with results presented by Walker & Tiederman (1990).

3.4.3. *Reynolds stress production*

It is interesting to compare the production of the three non-zero Reynolds stresses in water and drag-reduced flows. This comparison is based on the Reynolds transport equations given by Bradshaw (1978).

The transport equation for the streamwise normal-stress, $\overline{u^2}$ is

$$0 = \overset{\text{I}}{-2\overline{uv}\frac{\partial\overline{U}}{\partial y}} + \overset{\text{II}}{2\overline{\frac{p'}{\rho}\left(\frac{\partial u}{\partial x}\right)}} - \overset{\text{III}}{\frac{\partial}{\partial y}\overline{(u^2 v)}} + \overset{\text{IV}}{\nu\frac{\partial^2\overline{u^2}}{\partial y^2}} - \overset{\text{V}}{2\nu\left[\overline{\left(\frac{\partial u}{\partial x}\right)^2} + \overline{\left(\frac{\partial u}{\partial y}\right)^2} + \overline{\left(\frac{\partial u}{\partial z}\right)^2}\right]}. \tag{14}$$

The production of $\overline{u^2}$ is the first term on the right hand side. Term II is the 'pressure-strain' which tends to make the turbulence more isotropic by equalizing the normal stresses and reducing the shear stresses. Terms III and IV account for the transport of Reynolds stresses by turbulent velocity and viscous action respectively and term V represents the destruction of $\overline{u^2}$ through viscous fluctuations. Term I is balanced primarily by the destruction due to viscous fluctuations (term V) and the redistribution to the other stresses through the pressure-strain term (term II). The transport equation for the wall-normal normal stress $\overline{v^2}$ is shown as equation (15).

$$0 = \overset{\text{I}}{2\overline{\frac{p'}{\rho}\left(\frac{\partial v}{\partial y}\right)}} - \overset{\text{II}}{\frac{\partial\overline{v^3}}{\partial y}} - \frac{2}{\rho}\frac{\partial}{\partial y}\overline{(p'v)} + \overset{\text{IV}}{\nu\frac{\partial^2\overline{v^2}}{\partial y^2}} - \overset{\text{V}}{2\nu\left[\overline{\left(\frac{\partial v}{\partial x}\right)^2} + \overline{\left(\frac{\partial v}{\partial y}\right)^2} + \overline{\left(\frac{\partial v}{\partial z}\right)^2}\right]}. \tag{15}$$

For $\overline{v^2}$, there is no production term. The major source term is the pressure-strain correlation (term I) which increases $\overline{v^2}$ by extracting energy from $\overline{u^2}$. This source is
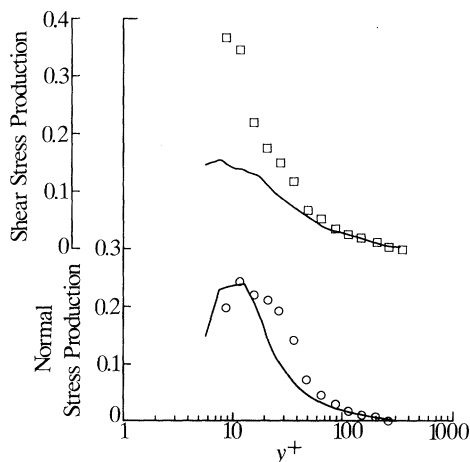
Figure 11. Productions profiles for the typical drag-reduced flow: ○, normal stress; □, shear stress; ——, fit to water data at equal τ_{w}.
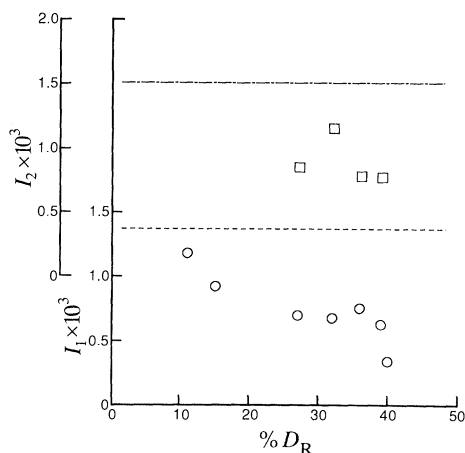
Figure 12. Variation of integrated production profiles with drag reduction; – – – –, average shear stress production of water flows; —·—, average normal stress production of water flows.

balanced primarily by the viscous destruction term (term V). Therefore, in this study, all normal Reynolds stresses are created from energy extracted from the $\overline{u^2}$ stress.

Finally, the transport equation for the Reynolds shear stress, $\overline{uv}$, is:

$$0 = \underset{\text{I}}{-\overline{v^2}\frac{\partial \bar{U}}{\partial y}} + \underset{\text{II}}{\frac{\overline{p'}}{\rho}\left(\frac{\partial u}{\partial y}+\frac{\partial v}{\partial x}\right)} - \underset{\text{III}}{\frac{\partial}{\partial y}\overline{(uv^2)}} - \underset{\text{IV}}{\frac{1}{\rho}\left(\frac{\partial}{\partial x}\overline{(p'v)}+\frac{\partial}{\partial y}\overline{(p'u)}\right)}$$

$$+ \underset{\text{V}}{\nu\frac{\partial^2 \overline{uv}}{\partial y^2}} - 2\nu\left[\underset{\text{VI}}{\left(\overline{\frac{\partial u}{\partial x}\frac{\partial v}{\partial x}}\right)+\left(\overline{\frac{\partial u}{\partial y}\frac{\partial v}{\partial y}}\right)+\left(\overline{\frac{\partial u}{\partial z}\frac{\partial v}{\partial z}}\right)}\right]. \quad (16)$$

As in equation (14), the major production term for $\overline{uv}$ is term I. Spalart (1988) points out that the pressure-strain term (term II) is primarily responsible for destruction of the shear stress, while the viscous dissipation term (term VI) accounts for very little destruction.

Figure 11 shows a comparison between the production terms for both the normal and Reynolds stresses for the typical drag-reduced flow and the equal wall shear water flow. The normal-stress production peak in the drag-reduced flow has shifted outward from the wall and has broadened because the average mean velocity and $\mathrm{d}\bar{U}/\mathrm{d}y$ have increased in the region $10 < y^+ < 100$. The same behaviour explains the increase in the Reynolds stress production.

Figure 12 displays the integrated production profiles normalized by the average velocity as a function of drag reduction. The quantities I_1 and I_2 are given by

$$I_1 = U_{\mathrm{avg}}^{-3}\int_0^a \overline{uv}\frac{\mathrm{d}\bar{U}}{\mathrm{d}y}\mathrm{d}y \quad \text{and} \quad I_2 = U_{\mathrm{avg}}^{-3}\int_0^a \overline{vv}\frac{\mathrm{d}\bar{U}}{\mathrm{d}y}\mathrm{d}y. \quad (17)$$

The dashed line is the average value of the integrated production profiles for water
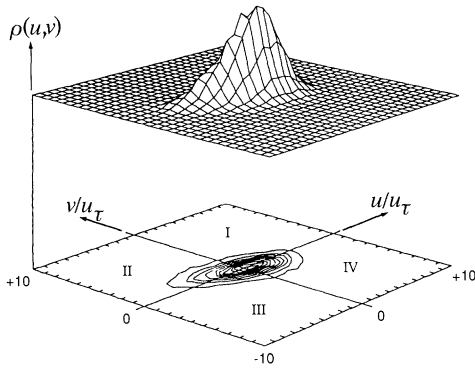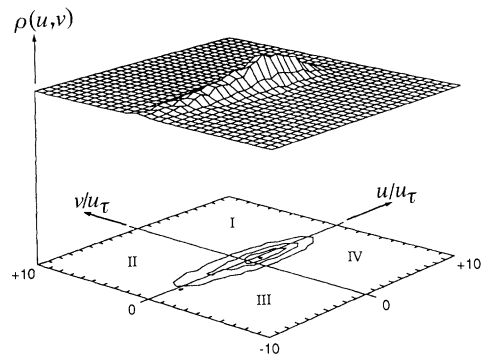
Figure 13

Figure 14

Figure 13. Probability of occurrence for a *uv* event at $y^+ = 37$ for the water flow at a wall strain rate of 2500 s^{-1}.

Figure 14. Probability of occurrence for a *uv* event at $y^+ = 38$ for the 4 p.p.m. flow at a wall strain of 2500 s^{-1}; $\% D_R = 39$.

flows in this Reynolds number range. It is clearly seen that turbulence production normalized with the average flow rate decreases with increasing drag reduction.

While the normal-stress production is lower in drag-reduced flows than it is in equal Reynolds number water flows, the levels of u'^+ are much higher across the channel while v'^+ is reduced. Equations (14) and (15), may explain this phenomenon. The viscous destruction for $\overline{v^2}$ (term V) in equation (15), is about the same as the destruction for the $\overline{u^2}$ (term V) in equation (14), because the dissipation scales are nearly isotropic. Therefore, to account for the increase in $\overline{u^2}$ and decrease in $\overline{v^2}$, transfer of energy from $\overline{u^2}$ to $\overline{v^2}$ through the pressure-strain correlation (the only other large term) must be inhibited. This explanation was first offered by Walker & Tiederman (1990), who point out that this is a valid explanation as long as the drag-reducing flows can be considered newtonian.

The drag-reduced flows also have lower integrated Reynolds stress production when normalized with the mean velocity. Walker & Tiederman (1990) show that for an inhomogeneous flow that the production of the Reynolds stress increases immediately downstream of the polymer injection. From these results, they concluded that the pressure-strain correlation causes increased destruction of the Reynolds stress. The present results suggest that in a homogeneous flow, since both the production of the Reynolds shear stress and the Reynolds shear stress are decreased, term II in equation (16) may not be any larger than in a water flow at equal Reynolds number.

Figures 13 and 14 show the probability of occurrence of a *uv* event for the cases of a wall strain rate of 2500 s^{-1} and well-mixed polymer concentrations of 0 and 4 p.p.m. respectively. It is readily seen that the occurrence of small-amplitude *uv* events are damped in the 4 p.p.m. flow while the large amplitude events remain unaffected. These results confirm Luchik & Tiederman's hypothesis that the small amplitude events are damped in drag-reduced flows while the large amplitude events are unaffected.

Figures 13 and 14 also reveal that the axes of principal stress are rotated from $\pm 45°$ toward the streamwise and wall-normal directions. This rotation yields the lower correlation coefficients displayed in figure 10. As noted by Schmid (1984),

Walker & Tiederman (1990), Gampert & Yong (1990) and Gyr & Bewersdorff (1990) this rotation is a common feature of drag-reducing flows.

4. Conclusions

Results from the factorial design clearly show that drag reduction depends upon wall strain rate, average polymer concentration, and channel height independently.

For this polymer-solvent combination, the slope of the logarithmic region of the mean velocity profile changes with the amount of drag reduction. Therefore, scale-up techniques based on constant slope can not be used.

The average shear stress and the local shear stress, which is independent of the channel's aspect ratio, were significantly different for all flows. The average shear stress was consistently 10–25 % higher than the local shear stress. For the Reynolds number range of $14\,000 < Re_h < 40\,000$, the difference between the averaged shear stress and the local shear stress increases with Reynolds number.

In six drag-reducing flows, the sum of the viscous and Reynolds stresses yielded the total shear stress. However, for the combination of highest wall strain rate $(4000\ \mathrm{s}^{-1})$, highest polymer concentration (5 p.p.m.) and smallest channel height (2.5 cm), the results were similar to those of Willmarth *et al.* (1987). In the outer flow the viscous and Reynolds stresses added to the total stress, $\tau_{\mathrm{w}}(1 - y/a)$. However, for $y^+ < 100$, the sum of the viscous and Reynolds stresses did not add up to the total stress, $\tau_{\mathrm{w}}(1 - y/a)$.

Turbulent shear stress levels in the polymer flow were not significantly different in drag-reduced flows (except for the special case mentioned previously) than in water flows at equal wall shear stress. The correlation coefficient in the drag-reduced flows was significantly lower across the channel than that of the equal wall shear stress water flow because the axes of principal stress rotate from $\pm 45°$ to the streamwise and wall-normal directions as drag reduction occurs.

No Reynolds number dependence was observed for the turbulent quantities in the near-wall region $(y^+ < 50)$ of the water flows. Inner scaling was appropriate for all turbulent quantities for the newtonian near-wall regions.

The integrated production profiles of $\overline{u^2}$ are lower in drag-reduced flows than in water flows when normalized with mass average velocity. However, the u' levels in drag-reduced flows were much higher than those in water flows at equal wall shear stress while v' was reduced in the drag-reduced flows. Since v' derives its energy from u' through the pressure-strain term, it is hypothesized that the polymer affects the transmission of energy through this mechanism.

The decrease in small-amplitude uv motions in polymer flow while the large amplitude uv motions remain unaffected when compared to equal wall shear stress water flow supports the findings of Luchik & Tiederman (1988). Since the larger uv motions are closely associated with the burst and sweep process on a one-to-one basis, the results also suggest that the burst rate from a streak in a low concentration drag-reduced flow is the same as that from a water flow at equal wall shear stress.

References

Berman, N. S. 1978 Drag reduction by polymers. *A. Rev. Fluid Mech.* **10**, 47.

Bradshaw, P. 1978 *Topics in applied physics*, vol. 12. *Turbulence*, p. 25. Springer-Verlag.

Coles, D. E. 1968 The young person's guide to the data. In *Computation of turbulent boundary layers – 1968* (ed. D. E. Coles & E. A. Hirst), p. 1. Stanford University.

Finnicum, D. S. & Hanratty, T. J. 1985 Turbulent normal-velocity fluctuations close to a wall. *Phys. Fluids* **28**, 1654.

Gampert, B. & Yong, C. K. 1990 The influence of polymer additives on the coherent structure of turbulent channel flow. In *Structure of turbulence and drag reduction* (ed. A. Gyr), p. 223. Springer-Verlag.

Granville, P. S. 1985 A method for predicting additive drag reduction from small-diameter pipe flows. *U.S. Navy report DTNSRDC/SPD-1142-01*.

Gyr, A. & Bewersdorft, H.-W. 1990 Changes of structure close to the wall of a turbulent flow in drag-reducing fluids. In *Structure of turbulence and drag reduction* (ed. A. Gyr), p. 215. Springer-Verlag.

Harder, K. J. 1989 Effect of wall strain rate, polymer concentration and channel height upon drag reduction and turbulent structure. MSME thesis, Purdue University.

Hunter, J. S. 1960 Some applications of statistics to experimentation. *AIChE Jl* **56**, 10.

Hussain, A. K. M. F. & Reynolds, W. C. 1975 Measurements in fully developed turbulent channel flow. *J. Fluids Engng* **97**, 568.

Kim, J., Moin, P. & Moser, R. 1987 Turbulence statistics in fully developed channel flow at low Reynolds number. *J. Fluid Mech.* **177**, 133.

Kline, S. J. 1990 Quasi-coherent structures in the turbulent boundary layer. I. Status report of a community-wide summary of the data. In *Near wall turbulence* (ed. S. J. Kline & N. H. Afghan), p. 200. New York: Hemisphere.

Kline, S. J. & Robinson, S. K. 1990 Turbulent boundary layer structure: progress, status and challenges. In *Structure of turbulence and drag reduction* (ed. A. Gyr), p. 3. Springer-Verlag.

Kreplin, H. & Ecklemann, H. 1979 Behavior of the three fluctuating velocity components in the wall region of a turbulent channel flow. *Phys. Fluids* **22**, 1233.

Luchik, T. S. & Tiederman, W. G. 1988 Turbulent structure in low concentration drag-reducing channel flows. *J. Fluid Mech.* **190**, 241.

Lumley, J. L. & Kubo, I. 1985 Turbulent drag reduction by polymer additives. In *The influence of polymer additives on velocity and temperature fields* (ed. B. Gampert), p. 3. Springer-Verlag.

McComb, W. D. & Rabie, L. H. 1982 Local drag reduction due to injection of polymer solutions into turbulent flow in a pipe. I. Dependence on local polymer concentration. II. Laser-Doppler measurements of turbulent structure. *AIChE Jl* **28**, 547.

Motier, J. F. & Carrier, A. M. 1989 Recent studies on polymer drag reduction in commercial pipelines. In *Drag reduction in fluid flows* (ed. R. H. J. Sellin & R. T. Moses), p. 197.

Reischman, M. M. & Tiederman, W. G. 1975 Laser Doppler anemometer measurements in drag-reducing channels flows. *J. Fluid Mech.* **70**, 369.

Robinson, S. K. 1991 Coherent motions in the turbulent boundary layer. *A. Rev. Fluid Mech.* **23**, 601.

Schmid, A. 1984 Experimental investigation of the influence of drag-reducing polymers on a turbulent channel flow. In *Drag reduction* (ed. R. H. J. Sellin & R. T. Moses), p. 12. University of Bristol.

Spalart, P. R. 1988 Direct simulation of a turbulent boundary layer up to $Re_0 = 1400$. *J. Fluid Mech.* **187**, 61.

Sreenivasan, K. R. 1989 The turbulent boundary layer. In *Frontiers in experimental fluid mechanics* (ed. M. Gad-el-Hak), p. 159. Springer-Verlag.

Tiederman, W. G. 1990 Review: the effect of dilute polymer solutions in viscous drag and turbulence structure. In *Structure of turbulence and drag reduction* (ed. A. Gyr), p. 187. Springer-Verlag.

Tiederman, W. G., Luchik, T. S. & Bogard, D. G. 1985 Wall layer structure and drag reduction. *J. Fluid Mech.* **156**, 419.

Virk, P. S. 1975 Drag reduction fundamentals. *AIChE Jl* **21**, 625.

Walker, D. T. & Tiederman, W. G. 1990 Turbulent structure and mass transport in a channel flow with polymer injection. *J. Fluid Mech.* **218**, 377.

Wei, T. & Willmarth, W. W. 1989 Reynolds number effects on the small scale structure of a turbulent channel flow. *J. Fluid Mech.* **204**, 57.

Wells, C. S. & Spangler, J. G. 1967 Injection of drag−reducing fluid into a turbulent pipe flow of a newtonian fluid. *Phys. Fluids* **10**, 1890.

Willmarth, W. W., Wei, T. & Lee, C. O. 1987 Laser anemometer measurements of Reynolds stress in a turbulent channel flow with drag reducing polymer additives. *Phys. Fluids* **30**, 933.

Wu, J. & Tulin, M. P. 1972 Drag reduction by ejecting additive solutions into purewater boundary layer. *J. basic Engng* **74**, 749.